BOHR International Journal of Engineering
2023, Vol. 2, No. 1, pp. 43–54
DOI: 10.54646/bije.2023.17
www.bohrpub.com

METHODS

Surrogate safety measures using bicycle vehicle models

Pushkin Kachroo[1*], K. Ramachandra Rao[2] and Geetam Tiwari[3]

[1]Departmet of Electrical and Computer Engineering, University of Nevada Las Vegas (UNLV), Las Vegas, NV, United States
[2]Department of Civil Engineering and TRIPC, Indian Institute of Technology, New Delhi, India
[3]Transportation Research and Injury Prevention Centre (TRIPC), Indian Institute of Technology, New Delhi, India

***Correspondence:**
Pushkin Kachroo,
pushkin@unlv.edu

Received: 26 September 2023; **Accepted:** 08 November 2023; **Published:** 15 December 2023

Surrogate Safety Measures (SSM) allow for analysis of crashes without having access to actual crash data as those are difficult to obtain, being of rare event nature. This article, for the first time, uses kinematic and dynamic bicycle models for vehicles for trajectory analysis to compute surrogate safety measures. The model has two versions, with and without the consideration of adhesion coefficients depending on the road conditions. Previously, only longitudinal models have been used and recently, a combined longitudinal and lateral model has been used by the authors but with a single wheel model, which is being enhanced by using the bicycle model in this paper.

Keywords: safety, surrogate, vehicle dynamics, lateral dynamics, adhesion, wheel slip

1. Introduction

1.1. Background

However, Traffic safety is a serious concern when we look at the aggregate annual data for example for a city. Hence, it is important to obtain data on accidents and fatalities so that we can design measures to counter unsafe conditions and behaviors. Since, crashes are rare events, we can use other safety surrogates that are not as rare and can act as proxy for the crash information.

Traffic accidents can be considered to be rare events in the normal driving on roads (1, 2). For instance, a study (3) shows that during 2016−2017, the fatality crash rate per 100 million miles driven for the age group 45−64 was 1.72. Similar numbers in terms of distance traveled or time spent traveling and accident or fatality rates show that actual accidents are rare compared to distance driven or time spent driving by an individual.

Analysis of vehicle and pedestrian trajectories can provide Surrogate Safety Measures (SSM), such as the measure Time to Collision (TTC) including some modifications of it. Some modifications are Time exposed time to collision (TET), and its integrated version Time integrated time to collision (TIT). Some other measures include delta-V (AV), relative speeds based, accelerations based, and various others (4, 5).

1.2. Research gap and contribution

Traditionally, the SSMs are calculated at an instant of time assuming that the vehicle will continue with the same current linear speed while ignoring the current angular speed. Some even use the current linear acceleration to extrapolate the movement till a crash within a time frame (6, 7).

False positive and false negative outcomes can be obtained for crash analysis if we ignore rotational motion of vehicles (8, 9). Hence, it is very important to perform rotational motion analysis as well. One-wheel or point model based kinematic analysis (8) and adhesion coefficient based one-wheel dynamic analysis has been performed (9) to enhance the modeling.

This paper improves upon the one-wheel or point-based models by utilizing bicycle models for vehicle trajectory generation.

2. Problem statement

Traffic video data taken using drone videos or videos placed at some fixed location, or even on vehicles, etc., can be processed to obtain trajectories of various trajectories. These trajectories typically give data in (x, y) coordinates with respect to time for vehicles as well as pedestrians in the videos. These trajectories can be processed to perform safety analysis by estimating the surrogate safety measures.

2.1. Road description

The road surface is shown as a parametrized surface in Figure 1 and the vehicle trajectory is shown as a subset of that surface as a one-dimensional parameterized curve. The two-dimensional surface can be parametrized in its three-dimensional background space as shown by

$$s = \{(x(u, v), y(u, v), z(u, v)) \,|u \in [a, b], v \in [c, d]\} \tag{1}$$

The indicator function demonstrates the bi-directionality of the road as shown in Eq. 2.

$$d(u, v) : [a, b] \times [c, d] \to \{l, r\} \tag{2}$$

We can now synthesize the surface description and also include the direction indicating variable to produce a single vector function shown in Eq. 3.

$$s_d = \{(x(u, v), y(u, v), z(u, v), d(u, v)) \,|u \in [a, b], v \in [c, d]\} \tag{3}$$

2.2. Trajectory description

Vehicle trajectories are used for performing SSM analysis to assess the closeness to a crash. Vehicle trajectories are curves that we parametrize using t to represent time, and representing the trajectory as $(u(t), v(t)), t \in [e, f]$. Subsets of trajectories close to each other are utilized for analysis of conflicts.

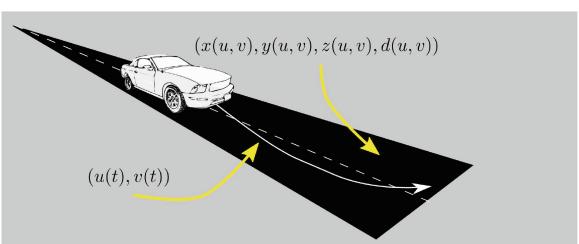

FIGURE 1 | Road surface and rrajectories.

3. Kinematic bicycle vehicle models

In this section we perform kinematic analysis which represents vehicle motion with velocities as inputs and outputs without utilizing or modeling forces. Adhesion coefficients are modeled in dynamic models that also incorporate forces as presented in section 5 "Dynamic analysis."

In the kinematic model, we have constraints on the velocity of the wheels. The constraint is that the wheels do not slide sideways and only have rotation in the direction they face. However, there are no constraints on the state the vehicle can reach. Hence, these velocity constraints are not integrable; otherwise, their integration would produce constraints on position and orientation, which does not exist. Non integrable velocity constraints make these systems non-holonomic.

We will now derive the ordinary differential equation model for a rear-wheel-drive front-wheel steering vehicle and a front-wheel-drive and front-wheel-steering vehicle using the non-holonomic constraints.

3.1. Kinematic bicycle model for rear-wheel-drive front-wheel-steering vehicle

Consider Figure 2 for the rear-wheel-drive front-wheel-steering vehicle. The real wheel's position is at (x, y) coordinates in the world frame. The wheel is at an angle of θ with the x axis. Let us denote the coordinates of the front wheel by (x_f, y_f). The non-holonomic constraints on the rear and front wheels can be written as equations by noting that the velocity normal to the wheels is zero. Hence, we have

$$\begin{aligned} \dot{x} \sin\theta - \dot{y} \cos\theta &= 0 \\ \dot{x_f} \sin(\theta + \delta) - \dot{y_f} \cos(\theta + \delta) &= 0 \end{aligned} \tag{4}$$

The relationship between (x_f, y_f) and (x, y) is as follows.

$$\begin{aligned} x_f &= x + l\cos\theta \\ y_f &= y + l\sin\theta \end{aligned} \tag{5}$$

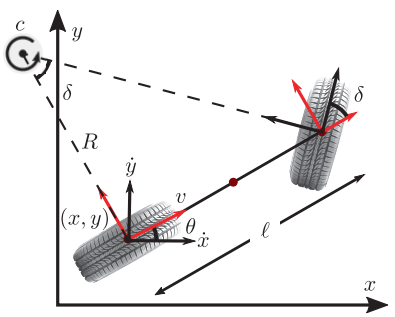

FIGURE 2 | Kinematic model for rear wheel drive front wheel steering vehicle.

Differentiating Eq. 5 and substituting in Eq. 4 gives

$$\begin{aligned} \dot{x}\sin\theta - \dot{y}\cos\theta &= 0 \\ \dot{x}_f\sin(\theta+\delta) - \dot{y}_f\cos(\theta+\delta) - \dot{\theta}l\cos\delta &= 0 \end{aligned} \tag{6}$$

We can write this in a matrix form $P\dot{V} = 0$, where P is the Pfaffian constraint matrix (10).

$$\begin{bmatrix} \sin\theta & -\cos\theta & 0 & 0 \\ \sin(\theta+\delta) & -\cos(\theta+\delta) & -l\cos\delta & 0 \end{bmatrix} \begin{bmatrix} \dot{x} \\ \dot{y} \\ \dot{\theta} \\ \dot{\delta} \end{bmatrix} = \begin{bmatrix} 0 \\ 0 \end{bmatrix} \tag{7}$$

The velocity vector $\dot{V} = \left[\dot{x}, \dot{y}, \dot{\theta}, \dot{\delta}\right]'$ belongs to the null space of the Pfaffian matrix P. The ordinary differential equations for this kinematic model can be directly derived now from **Figure 2**, and the null space condition then can be confirmed from that model.

The main point to understand in the derivation is that since both wheels are purely rotating, the common center of rotation has to be perpendicular to both wheels. **Figure 2** shows the instantaneous center of rotation as point c, which is the intersection point for the perpendicular lines from both wheels. The two inputs are linear speed v of the rear wheel, and angular steering rate $\omega = \dot{\delta}$ of the front wheel.

From **Figure 2**, we can easily see that $\dot{x} = v\cos\theta$ and $\dot{y} = v\sin\theta$. Because c is the instantaneous center of rotation, we have $\dot{\theta} = v/R$. Using the right-angled triangle in **Figure 2**, we see that $R = l/\tan\delta$. Finally, as mentioned before, we have $\omega = \dot{\delta}$. We can summarize the system as

$$\begin{bmatrix} \dot{x} \\ \dot{y} \\ \dot{\theta} \\ \dot{\delta} \end{bmatrix} = \begin{bmatrix} \cos\theta \\ \sin\theta \\ \tan\delta/l \\ 0 \end{bmatrix} v + \begin{bmatrix} 0 \\ 0 \\ 0 \\ 1 \end{bmatrix} \omega \tag{8}$$

We can see clearly that the model has a singularity at $\delta = \pm\pi/2$ because of the tan term. This is physically also visible since when the front wheel is turned to any of these angles, the front wheel won't allow motion perpendicular to it, while the back wheel has only that direction possible, creating a singularity.

3.2. Kinematic bicycle model for front-wheel-drive front-wheel-steering vehicle

Consider **Figure 3** for the front-wheel-drive front-wheel-steering vehicle. The front wheel's position is at (x, y)

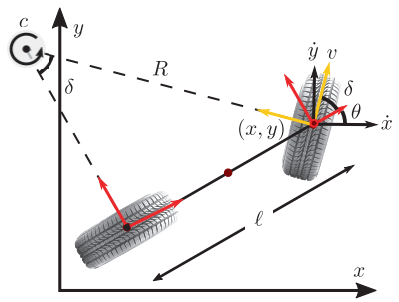

FIGURE 3 | Kinematic model for front-wheel-drive front-wheel-steering vehicle.

coordinates in the world frame. The rear wheel is at an angle of θ with the x axis, while the front wheel's steering angle is δ. Let us denote the coordinates of the rear wheel by (x_r, y_r). The non-holonomic constraints on the rear and front wheels can be written as equations by noting that the velocity normal to the wheels is zero. Hence, we have

$$\begin{aligned} \dot{x}\sin(\theta+\delta) - \dot{y}\cos(\theta+\delta) &= 0 \\ \dot{x}_r\sin\theta - \dot{y}_r\cos\theta &= 0 \end{aligned} \tag{9}$$

The relationship between (x_f, y_f) and (x, y) is as follows.

$$\begin{aligned} x_r &= x - l\cos\theta \\ y_r &= y - l\sin\theta \end{aligned} \tag{10}$$

Differentiating Eq. 10 and substituting in Eq. 9 gives

$$\begin{aligned} \dot{x}\sin(\theta+\delta) - \dot{y}\cos(\theta+\delta) &= 0 \\ \dot{x}\sin\theta - \dot{y}\cos\theta + \dot{\theta}l &= 0 \end{aligned} \tag{11}$$

We can write this in a matrix form $PV = 0$, where P is the Pfaffian constraint matrix (10).

$$\begin{bmatrix} \sin(\theta+\delta) & -\cos(\theta+\delta) & 0 & 0 \\ \sin\theta & -\cos\theta & -l & 0 \end{bmatrix} \begin{bmatrix} \dot{x} \\ \dot{y} \\ \dot{\theta} \\ \dot{\delta} \end{bmatrix} = \begin{bmatrix} 0 \\ 0 \end{bmatrix} \tag{12}$$

The velocity vector $\dot{V} = \left[\dot{x}, \dot{y}, \dot{\theta}, \dot{\delta}\right]'$ belongs to the null space of the Pfaffian matrix P. The ordinary differential equations for this kinematic model can be directly derived now from **Figure 2**, and the null space condition then can be confirmed from that model.

The main point to understand in the derivation is that since both wheels are purely rotating, the common center of rotation has to be perpendicular to both wheels. **Figure 3** shows the instantaneous center of rotation as point c, which is the intersection point for the perpendicular lines from both wheels. The two inputs are linear speed v of the front wheel, and angular steering rate $\omega = \dot{\delta}$ of the front wheel.

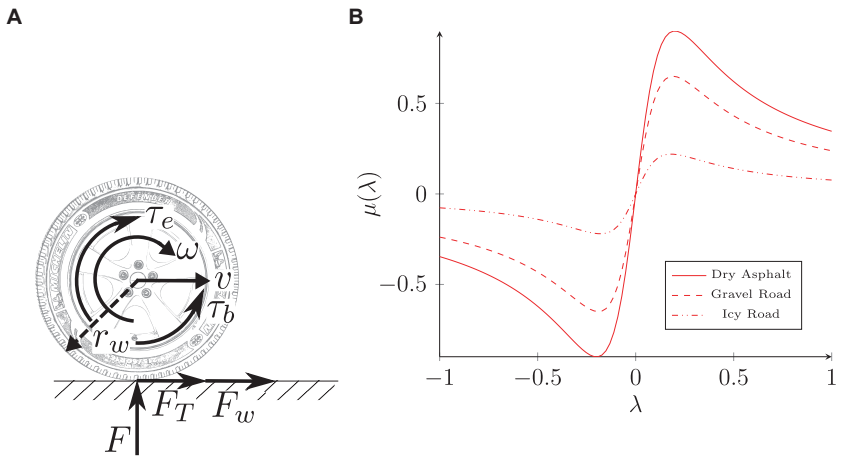

FIGURE 4 | Wheel dynamics and adhesion. **(A)** Wheel dynamics **(B)** Adhesion coefficient wheel slip relationship.

From **Figure 3**, we can easily see that $\dot{x} = v\cos(\theta + \delta)$ and $\dot{y} = v\sin(\theta + \delta)$. Because c is the instantaneous center of rotation, we have $\dot{\theta} = v/R$. Using the right-angled triangle in **Figure 3**, we see that $R = l/\sin\delta$ Finally, as mentioned before, we have $\omega = \dot{\delta}$. We can summarize the system as

$$\begin{bmatrix} \dot{x} \\ \dot{y} \\ \dot{\theta} \\ \dot{\delta} \end{bmatrix} = \begin{bmatrix} \cos(\theta + \delta) \\ \sin(\theta + \delta) \\ \sin\delta/l \\ 0 \end{bmatrix} v + \begin{bmatrix} 0 \\ 0 \\ 0 \\ 1 \end{bmatrix} \omega \tag{13}$$

Since the tan term in the rear-wheel-drive model has been replaced by the sin term, the singularity that was present in that model has been removed. This can also be seen physically as only the front wheel will have the speed v and the motion at angle $\pm\pi/2$ will be enabled.

4. Controllability analysis for kinematic bicycle model

As the analysis in this paper is concerned with traffic safety and specifically with vehicle trajectories for the sake of assessing the probability of crashes, controllability of a vehicle is an important aspect of the analytical framework. Hence, we take up this topic for further study.

4.1. Controllability

The following definitions are for a system given by

$$\dot{x} = f(x, u), x(0) = x_0 \in \mathbb{R}^n \tag{14}$$

Definition 1 (Reachability). A state x_f is reachable from state x_i if there exists time *instances* t_i *and* t_f *and a function* $u(\cdot)$, such that *a solution* $x(\cdot)$ *exists to the system given by Eq. 14 such that*$x(t_i) = x_i$, *and*$x(t_f) = x_f$.

Definition 2 (Controllability). *A system given by Eq. 14 is called controllable if any given state*$_{x_f}$ *is reachable from any other given state* $_{x_i}$.

Definition 3 (Local Controllability). *A system given by Eq. 14 is called locally controllable* (11) *at* x_0 *and* T *if*$\forall_\in > 0, \exists\delta, 0 < \delta \leq \varepsilon$, *such that* $\forall x_a \in B(x_0, \delta), x_b \in B(x_0, \delta), \exists u(\cdot)$ *to enable* $x(0) = x_a$ *and* $x_b = x(T)$ *while* $\forall t \in (0, T), x(t) \in B(x_0, \varepsilon)$.

4.1.1. Controllability for linear time invariant (LTI) systems

For a linear system

$$\dot{x} = Ax + Bu \tag{15}$$

with$x \in \mathbb{R}^n$, $u \in \mathbb{R}^m$, $A \in M(n, m)$, where $M(n, m)$ is a real-valued matrix of size $M \times n$, controllability condition is given by Theorem 1 (12).

Theorem 1 (Controllability for LTI Systems). *The system of Eq. 15 is controllable if*

$$rank[B, AB, A^2B, \cdots, A^{n-1}B] = n \tag{16}$$

is satisfied.

4.1.2. Controllability for nonlinear systems

For a nonlinear system

$$\dot{x} = f(x, u) \tag{17}$$

with $x \in \mathbb{R}^n$, $u \in \mathbb{R}$, and $f(x, u) \in \mathbb{R}^n$, local controllability condition is given by Theorem 2 (11).

Theorem 2 (Local Controllability for nonlinear Systems about equilibrium). Consider the system of Eq. 17. Let $f(x, u)$ be continuously differentiable about (x_e, u_e) called the equilibrium, where

$$f(x_e, u_e) = 0 \tag{18}$$

Let $A = f_x(x_e, u_e)$and $B = f_u(x_e, u_e)$, then if the linearization of Eq. 17 given by Eq. 15 is controllable, then the system of Eq. 17 is locally controllable about (x_e, u_e).

For the stability of a drift-free nonlinear finite-dimensional dynamical system, we can use the theory of Lie brackets and Lie algebra.

Definition 4 (Lie Bracket). *Lie bracket* $[f, g]$ *of two vector fields* $f(x) : \mathbb{R}^n \to \mathbb{R}^n$ and $g(x) : \mathbb{R}^n \to \mathbb{R}^n$ *is given by*

$$[f, g](x) = f_x(x)\, g(x) - g_x(x) f(x) \tag{19}$$

where $f_x(x)$ *and* $g_x(x)$ *are the Jacobian matrices of* $f(x)$ *and* $g(x)$.

Consider the drift free system

$$\dot{x} = \sum_{i=1}^{m} f_i(x)\, u_i \tag{20}$$

Create recursive sets as follows.

$$\begin{gathered} L_0 = \{f_i\}\ i,\ u_i \in \mathbb{R} \\ L_j = L_{j-1} \cup \{[f, g]\}, f \in L_0,\ g \in L_{j-1}, j = 1, 2, \cdots \\ \text{rank} L = n\, \text{rank} L_{j-1} \end{gathered} \tag{21}$$

Let L be the set L_j with the minimum value of j such that $\text{rank}L_j = \text{rank}L_{j-1}$, where the rank operator means the rank of the vector space spanned by the members of the set.

Theorem 3 (Local Controllability for nonlinear drift-free Systems). *Consider the drift-free nonlinear system of Eq. 20 where for each* i, $u_i \in \mathbb{R}$, *the system is locally controllable about the origin if* $\text{rank}L = n$. (13, 14).

Although controllability analysis of a system like this has been performed (10), it has never been done in the context of trajectory analysis for surrogate safety measures. Hence, we present those results as they relate to traffic safety.

4.2. Controllability for kinematic bicycle model for rear-wheel-drive front-wheel-steering vehicle

The kinematic model for the kinematic bicycle model for rear-wheel-drive front-wheel-steering vehicle is given in Eq. 22, and can be represented as

$$\dot{q} = \begin{bmatrix} \dot{x} \\ \dot{y} \\ \dot{\theta} \\ \dot{\delta} \end{bmatrix} = f_1(q)\, v + f_2(q)\, w = \begin{bmatrix} \cos\theta \\ \sin\theta \\ \tan\delta/\ell \\ 0 \end{bmatrix} v + \begin{bmatrix} 0 \\ 0 \\ 0 \\ 1 \end{bmatrix} w \tag{22}$$

This is a drift-free system, since when we make the two control variables equal to zero,

then $\dot{q} = 0$, implying that the system does not move, and hence, is drift free.

4.2.1. Controllability at a point

As the system is drift free, we see that every state of the system is an equilibrium point of the system. Let us denote by q_e any state of the system considered as a given equilibrium point so that we can study its stability.

4.2.1.1. Controllability for linearized system. The linearized dynamics about the given state q_e and zero input for the kinematic model are:

$$\dot{\tilde{q}} = f_1(q_e)\, v + f_2(q_e)\, \omega = \begin{bmatrix} f_1(q_e) & f_2(q_e) \end{bmatrix} \begin{bmatrix} v \\ \omega \end{bmatrix} = F(q_e)\, V \tag{23}$$

Here, $\tilde{q} = q - q_e$

We see that the $F(q_e)$ matrix in Eq. 23 has rank 2, and hence the system is not controllable. Hence, no linear control can stabilize the system even locally.

4.2.1.2. Controllability for the nonlinear system. For the stability of a drift-free nonlinear finite-dimensional dynamical system, we can use the theory of Lie brackets and Lie algebra. From Eq. 22, we see that

$$\begin{gathered} f_1 = \begin{bmatrix} \cos\theta \\ \sin\theta \\ \tan\delta/\ell \\ 0 \end{bmatrix},\ f_2 = \begin{bmatrix} 0 \\ 0 \\ 0 \\ 1 \end{bmatrix},\ [f_1, f_2] = \begin{bmatrix} 0 \\ 0 \\ -1/(\ell \cos^2\delta) \\ 0 \end{bmatrix}, \\ [f_1, [f_1, f_2]] = \begin{bmatrix} -\sin\theta/(\ell \cos^2\delta) \\ \cos\theta/(\ell \cos^2\delta) \\ 0 \\ 0 \end{bmatrix} \end{gathered} \tag{24}$$

We clearly see that rank $L = 4$and hence, the system is locally controllable at any state except at $\delta = \pm \pi/2$.

5. Dynamic analysis

Vehicle dynamics can be decoupled into longitudinal dynamics and lateral Dynamics. The dynamic analysis will essentially involve the modeling of vehicle and road interaction-based adhesion coefficient, which is then involved in producing tractive forces.

5.1. Longitudinal dynamics

In this subsection, we present the longitudinal wheel dynamics including the modeling of adhesion coefficient, and follow it with the modeling of longitudinal vehicle dynamics.

5.1.1. Wheel dynamics

Traction and braking forces that are produced because of the relative motion of the tire with respect to the ground cause

TABLE 1 | Notation for the free body diagram of a parked car.

Symbol	Meaning
r_w	Wheel radius
ω	Angular speed (Wheel)
v	Linear Speed (Vehicle)
ω_v	Normalized Vehicle Speed
τ_e	Wheel Engine Torque
τ_b	Braking torque
F_T	Tractive force
F_w w	Viscous friction (wheel)
F	Reaction force (normal, ground)
μ	Adhesion coefficient
λ	Wheel slip
J_w	Moment of inertia (wheel)

vehicle motion in terms of acceleration and deceleration. These forces are functions of wheel slip which quantifies the relative motion of the tire with respect to the ground, and is defined as

$$\lambda = \frac{\omega - \omega_v}{\text{Max}\,(\omega,\ \omega_v)}, \text{where } \omega_v = \frac{v}{r_\omega} \tag{25}$$

where ω is the tire angular velocity, v is the vehicle linear speed, r is the tire radius, and ω_v is the normalized vehicle linear velocity obtained by dividing the linear speed by the tire radius. **Figure 4A** shows the wheel dynamics as well as these associated variables. **Table 1** provides a summary of these variables, their symbols, and their meaning.

The product of the adhesion coefficient and the normal ground reaction force produces the tractive force for vehicle propulsion. The adhesion coefficient depends on wheel slip, which in turn is defined by Eq. 25. The condition for wheel slip to be positive is $\omega > \omega_v$, whereas the condition for wheel slip to be negative is $\omega < \omega_v$. **Figure 4a** shows how adhesion coefficient is a function of wheel slip. Positive wheel slip λ produces positive value of adhesion coefficient μ, which produces forward driving tractive force, which in turn produces acceleration. Similarly, positive wheel slip λ produces negative value of adhesion coefficient μ, which produces backward tractive force, which in turn produces deceleration. The negative traction os obtained when brakes are applied rendering a negative wheel slip, as in that case $\omega < \omega_v$.

Many researchers have obtained various approximate models for $\mu - \lambda$ relationship (15, 16). Some general models such as the Burckhardt's and Pacejka's models allow for much flexibility, consequently rendering it with too many parameters. We use a much simpler model for our purposes (17):

$$\mu\,(\lambda) = 2\mu_0 \frac{\lambda_0}{\lambda_0^2 + \lambda^2} \tag{26}$$

where μ_0 is the peak adhesion coefficient value obtained at a corresponding wheel slip of λ_0.

The different sets of $(\alpha_0, \alpha_1, \alpha_1)$ indicate different road conditions, such as normal, icy, etc. **Figure 4a** shows the $\mu - \lambda$ relationships for different road conditions. These different conditions were obtained by utilizing that the corresponding parameters which were, respectively, related to those different road conditions (15, 18).

Tractive force formula is

$$F_T = \mu\,(\lambda)\,F \tag{27}$$

The wheel angular acceleration is obtained as:

$$\dot{\omega} = \frac{d\omega}{dt} = \frac{1}{J_w}\left[\tau_e - \tau_b - r_w\,(F_T + F_w)\right] \tag{28}$$

The over dot on a symbol represents its time derivative.

5.1.2. Vehicle dynamics

Now we consider the longitudinal dynamics of a vehicle. Let us consider a rear drive vehicle as shown in **Figure 5**.

The dynamics for the vehicle are:

$$\dot{v} = \frac{dv}{dt} = \frac{1}{m}\left[F_T - F_v\right] \tag{29}$$

Balancing the moments of all forces about the front wheel, we obtain the following equation.

$$F_r = \frac{1}{\ell_f + \ell_r}\left[mg\ell_f + F_v h_a + m\,\dot{v}\,h\right] \tag{30}$$

Substituting Eq. 29 in Eq. 30 yields

$$F_r = \frac{1}{\ell_f + \ell_r}\left[mg\ell_f + F_v\left(h_a - h\right) + F_T h\right] \tag{31}$$

We have for tractive force

$$F_T = \mu\,(\lambda)\,F_r \tag{32}$$

Using Eq. 32 in Eq. 31 gives us the expression for F_T as

$$F_T = \frac{\mu\,(\lambda)}{\ell_f + \ell_r - \mu\,(\lambda)\,h}\left[mg\ell_f + F_v\left(h_a - h\right)\right] \tag{33}$$

The aerodynamic force F_v is generally quadratic and has the form $C_a v^2$. Hence, in summary, the overall vehicle dynamics are given by:

$$\dot{\omega} = \frac{d\omega}{dt} = \frac{1}{J_w}\left[\tau_e - \tau_b - r_w\,(F_T + F_w)\right]$$

$$\dot{v} = \frac{dv}{dt} = \frac{1}{m}\left[F_T - F_v\right] \tag{34}$$

$$\lambda = \frac{\omega - \omega_v}{\max\,(\omega,\ \omega_v)}, \text{ where } \omega_v = \frac{v}{r_\omega}$$

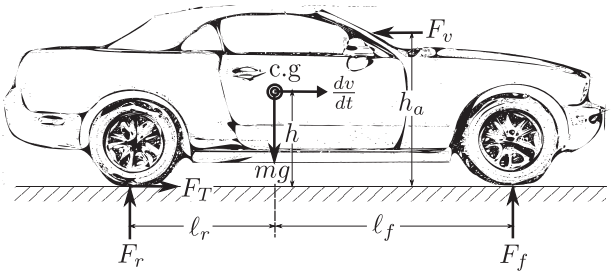

FIGURE 5 | Vehicle dynamics.

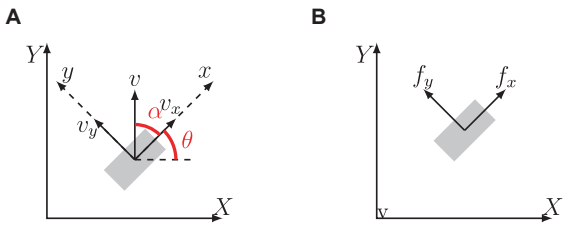

FIGURE 6 | Vehicle lateral dynamics. **(A)** Wheel dynamics **(B)** Wheel forces.

$$\mu(\lambda) = \mu(\lambda) = 2\mu_0 \frac{\lambda_0}{\lambda_0^2 + \lambda^2}$$

$$F_T = \frac{\mu(\lambda)}{\ell_f + \ell_r - \mu(\lambda) h} \left[mg\ell_f + F_v (h_a - h) \right]$$

$$F_v = C_a v^2, \text{and} F_w = C_v \omega$$

5.2. Lateral wheel dynamics

Figure 6a shows the lateral dynamics for the wheel. The coordinate frame for the wheel body is shown by (x, y), where (X, Y) indicates the world coordinates. The angle between the world X axis and vehicle x axis is the wheel yaw angle θ. The x component of the wheel velocity is v_x, while v_y is the y component of the wheel velocity. The angle between the x axis and the velocity vector, α, is the slip angle.

Forces on the wheel are shown in **Figure 6B**. The driving tractive force caused by adhesion is F_x, which is in the longitudinal direction. Lateral tractive force is indicated by F_y. Both these forces depend not only on wheel slip but also on the slip angle α. We use F for the normal reaction force to obtain

$$f_x = \mu_x(\lambda, \alpha) F, \quad f_y = \mu_y(\lambda, \alpha) F \tag{35}$$

A typical road condition plots of $\mu_x(\lambda, \alpha)$ and $\mu_y(\lambda, \alpha)$ are shown in **Figure 7**.

Different road conditions have correspondingly different plots as shown in **Figure 8**.

Very flexible formulae with a lot of parameters have been used for the two coefficients (16). However, we choose simplified models appropriate for our application given by

$$\mu_x(\lambda, \alpha) = 2\mu_0 \frac{\lambda_0}{\lambda_0^2 + \lambda^2} e^{-\alpha} \tag{36}$$

5.3. Combined longitudinal and lateral dynamics

In this subsection we present combined longitudinal and lateral dynamics. As before, the emphasis will be on road tire interaction with respect to adhesion, which will show its impact on both longitudinal as well as lateral motion. A two-axle bicycle model will be used for the derivation of the dynamics.

To develop the dynamics equations, we will use a moving frame that is attached to the vehicle body. It will be related to the fixed road inertial frame dynamically. We transform the dynamic equations to the vehicle moving frame and obtain (19, 20).

$$^V F = m^V a_v + m^V \omega_v \times {}^V V_v \tag{37}$$

We use the following notation in our model, $\omega_x = \omega_y = 0$, $\omega_z = \omega = \dot{\theta}$, $a_x = \ddot{x}$, $a_y = \ddot{y}$, $a_z = 0$, where an overhead dot symbol indicates differentiation of that variable with respect to time, and a double overhead dot indicates second derivative of that variable with respect to time. We can represent our model in component form as

$$\begin{aligned} \begin{bmatrix} F_x \\ F_y \\ F_z \end{bmatrix} &= m \begin{bmatrix} a_x \\ a_y \\ a_z \end{bmatrix} + m \begin{bmatrix} \omega_x \\ \omega_y \\ \omega_z \end{bmatrix} \times \begin{bmatrix} v_x \\ v_y \\ v_z \end{bmatrix} \\ = m \begin{bmatrix} a_x + \omega_y v_z - \omega_z v_y \\ a_y + \omega_z v_x - \omega_x v_z \\ a_z + \omega_x v_y - \omega_y v_x \end{bmatrix} &= m \begin{bmatrix} a_x - \omega v_y \\ a_y - \omega v_x \\ 0 \end{bmatrix} \end{aligned} \tag{38}$$

Figure 9a shows the vehicle/body coordinate system (x, y, θ) as well as the road/world coordinate system (X, Y, θ). It also shows the tire forces resolved in the x and y directions and shown as an upper case F, or in the case of front-steered wheel also resolved in the direction of the wheel and perpendicular to it and shown as a lower case f. The subscript show the resolution as x or y, and r refers to rear, whereas f refers to the front wheel. The steering angle is shown as δ.

Newton's laws are used to derive the ordinary differential equations for the dynamics. Eq. 38 is used for accelerations in the x and y directions. Then, we apply Newton's laws in the x and y directions, and by taking m as the vehicle mass results in the following equations.

$$\begin{aligned} m\ddot{x} &= m\dot{y}\dot{\theta} + F_{xr} + F_{xf} \\ m\ddot{y} &= m\dot{y}\dot{\theta} + F_{yr} + F_{yf} \end{aligned} \tag{39}$$

We use I_z for the vehicle moment of inertia about the center of gravity (c.g) in the z direction. We obtain the following

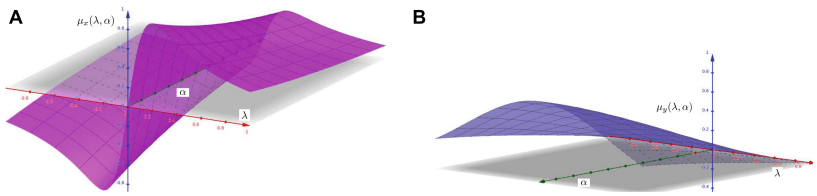

FIGURE 7 | Longitudinal and lateral adhesion coefficients. **(A)** $\mu_x(\lambda, \alpha)$ **(B)** $\mu_y(\lambda, \alpha)$

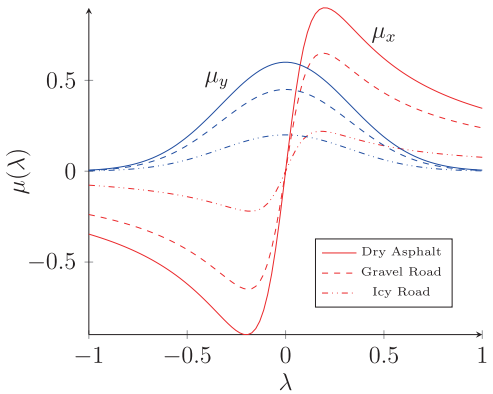

FIGURE 8 | Different road conditions.

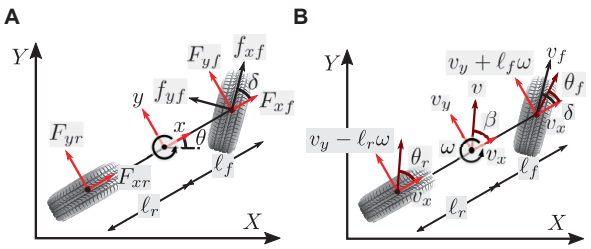

FIGURE 9 | Bicycle Model. **(A)** Forces **(B)** Side slip angles.

equations by taking moments about the c.g. and by applying rotational Newton's law.

$$I_z \ddot{\theta} = F_{yf}\ell_f - F_{yr}\ell_r \tag{40}$$

The axial forces F_{xf} and F_{yf} are obtained by a rotation of the steering angle δ as shown in Eq. 41.

$$\begin{bmatrix} F_{xf} \\ F_{yf} \end{bmatrix} = R_\delta \begin{bmatrix} f_{xf} \\ f_{yf} \end{bmatrix} = \begin{bmatrix} \cos\delta & -\sin\delta \\ \sin\delta & \cos\delta \end{bmatrix} \begin{bmatrix} f_{xf} \\ f_{yf} \end{bmatrix} \tag{41}$$

As the vehicle frame at any given time has an angle θ with respect to the ground frame, we can use rotation matrix to transform local velocity coordinates to the global ones.

$$\begin{bmatrix} \dot{X} \\ \dot{Y} \end{bmatrix} = R_\theta \begin{bmatrix} \dot{x} \\ \dot{y} \end{bmatrix} = \begin{bmatrix} \cos\theta & -\sin\theta \\ \sin\theta & \cos\theta \end{bmatrix} \begin{bmatrix} \dot{x} \\ \dot{y} \end{bmatrix} \tag{42}$$

Now, to obtain the tire forces f_{xf}, f_{yf}, f_{xr}, and f_{yr}, we need to consider **Figure 4A** as well as **Figure 9B**. Wheel rotational

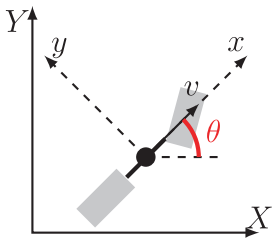

FIGURE 10 | Standard TTC setup.

dynamics are obtained as

$$\begin{aligned} I_{\omega f}\dot{\omega}_f &= T_f - f_{xf} r_{\omega f} \\ I_{\omega r}\dot{\omega}_r &= T_r - f_{xr} r_{\omega r} \end{aligned} \tag{43}$$

Wheel slip at each wheel is defined based on Eq. 25, except we use the wheel angular velocities, their respective radii, as well as their speed in the direction of the wheel.

$$\begin{aligned} \lambda_f &= \frac{\omega_f - \omega_{v_f}}{\max(\omega_f, \omega_{v_f})}, \text{ where } \omega_{v_f} = \frac{v_f}{r_{\omega_f}} \\ \lambda_r &= \frac{\omega_r - \omega_{v_r}}{\max(\omega_r, \omega_{v_r})}, \text{ where } \omega_{v_r} = \frac{v_r}{r_{\omega_r}} \end{aligned} \tag{44}$$

From **Figure 9B**, we see that (21).

$$\begin{aligned} \alpha_f &= \theta_f - \delta_f = \tan^{-1}\frac{v_y + \ell_f\omega}{v_x} - \delta \\ \alpha_r &= \theta_r = \tan^{-1}\frac{v_y + \ell_r\omega}{v_x} \end{aligned} \tag{45}$$

We can use the expressions that we have developed for tractive forces and the normal forces to obtain the front and rear wheel forces after ignoring the wind drag as

$$\begin{aligned} f_{xf} &= \mu_x(\lambda_f, \alpha_f) F_f = \mu_x(\lambda_f, \alpha_f) \frac{mg\ell_r - ma_x h}{\ell_f + \ell_r} \\ f_{yf} &= \mu_y(\lambda_f, \alpha_f) F_f = \mu_y(\lambda_f, \alpha_f) \frac{mg\ell_r - ma_x h}{\ell_f + \ell_r} \\ f_{xr} &= F_{xr} = \mu_x(\lambda_r, \alpha_r) F_r = \mu_x(\lambda_r, \alpha_r) \frac{mg\ell_f + ma_x h}{\ell_f + \ell_r} \\ f_{yr} &= F_{yr} = \mu_y(\lambda_r, \alpha_r) F_r = \mu_y(\lambda_r, \alpha_r) \frac{mg\ell_f + ma_x h}{\ell_f + \ell_r} \end{aligned} \tag{46}$$

6. SSM analysis

In this section we will develop the technique to obtain SSM using the developed bicycle models. Without loss of generality, we will use the Time to Collision (TTC) measure as the SSM for illustration purposes.

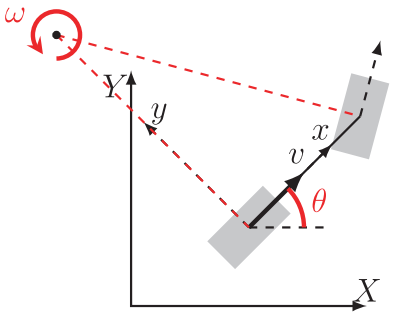

FIGURE 11 | Kinematic TTC setup.

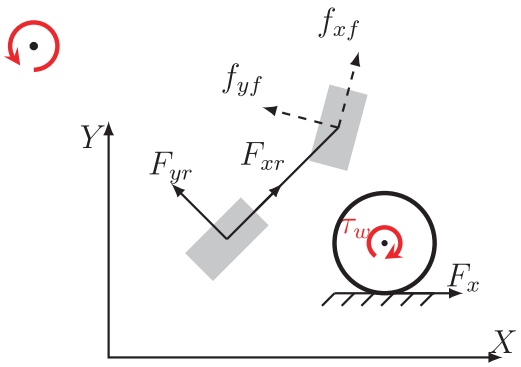

FIGURE 12 | Dynamic TTC setup.

6.1. Standard analysis

First-Order Model: In the traditional standard methods for SSM using TTC, it is assumed that at a given time whatever is the velocity of the vehicle, it will remain constant in the future. Based on this analysis, it is estimated whetehr a collision will take place or not, and if yes, then what is the time for collision.

Using **Figure 10**, we can see that even if the steering angle is not zero, or even if the vehicle is having angular velocity, those are ignored in the traditional standard methods, and the current velocity is used to extend the future vehicle locations. The figure shows the current (x, y) location of the vehicle with its current yaw angle of θ. Eq. 47 provides the dynamics in which angle θ will be a constant and the location (x, y) will move in the straight line with that fixed angle.

$$\begin{aligned} \dot{x} &= v \\ \dot{X} = v\cos\theta, \quad \dot{Y} &= v\sin\theta \end{aligned} \tag{47}$$

6.1.1. Second-order model

There are some models studied in the past (6) that use initial acceleration to be constant for calculating TTC. The equations for those second-order models are obtained by augmenting Eq. 47 with an additional differential equation $\dot{v} = a$, with a constant a. *As* compared to the previous model, the velocity can change (in magnitude but not in direction, i.e., the speed can change) but the direction of vehicle movement is still constant.

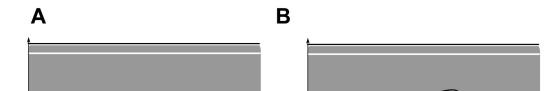

FIGURE 13 | Standard model for vehicle and an obstacle. **(A)** Collision case **(B)** Non-collision.

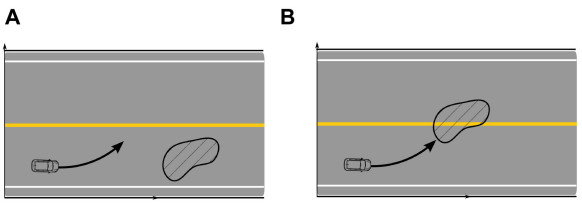

FIGURE 14 | Kinematic model for vehicle and an obstacle. **(A)** Collision case **(B)** Non-collision.

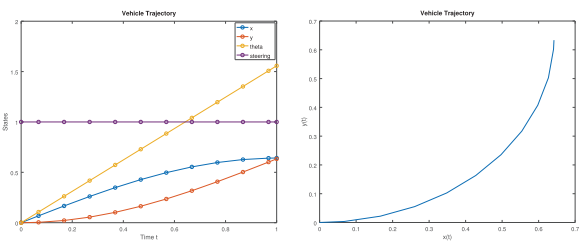

FIGURE 15 | Vehicle trajectory plots with angular rate and steering.

6.2. Bicycle kinematic analysis

6.2.1. First-order model

Eq. 8 shows the differential equations that provide the bicycle kinematic model for a vehicle that has its steering at the front and is driven by the rear wheels. At the time t for which TTC analysis has to be performed, in this model we keep the initial linear vehicle speed constant as well as the initial steering angle, as compared to the standard models that completely ignore the steering. With this assumption, the natural curved trajectory is produced as compared to the faulty straight one.

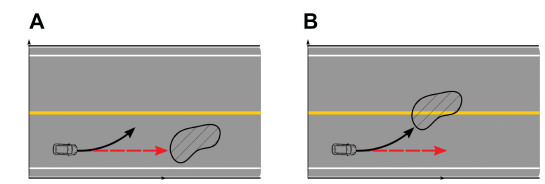

FIGURE 16 | Kinematic model for vehicle and an obstacle. **(A)** False positive **(B)** False negative.

The front steering rear wheel drive bicycle model kinematics can be seen in **Figure 11**. The figure shows the initial coordinates (x, y) with a yaw angle of θ. The vehicle

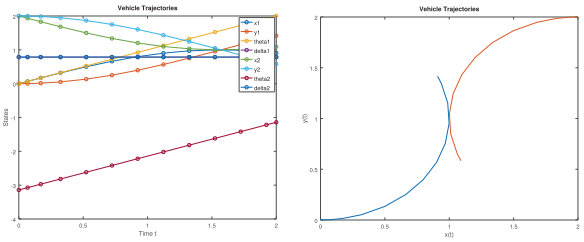

FIGURE 17 | Vehicle trajectory plots for interacting vehicles.

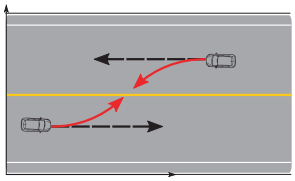

FIGURE 18 | Vehicle trajectories: false negative.

will be assumed to keep its initial linear velocity v as well as its initial angular velocity ω. The center of instantaneous rotation is obtained as the intersection point of the normal straight lines coming from the two wheels. This way there is no slipping of the wheels, and there is only pure rolling of the wheels. The curved trajectory obtained using Eq. 48 becomes obvious with this analysis.

$$\begin{bmatrix} \dot{x} \\ \dot{y} \\ \dot{\theta} \\ \dot{\delta} \end{bmatrix} = \begin{bmatrix} \cos\theta \\ \sin\theta \\ \tan\delta/\ell \\ 0 \end{bmatrix} v + \begin{bmatrix} 0 \\ 0 \\ 0 \\ 1 \end{bmatrix} \omega \qquad (48)$$

with $\omega = 0$.

Second-order model: We can convert the model given Eq. 48 into a second-order model easily. We have two inputs in that model, v and ω. We can convert any of these two or both into first-order models by adding the differential equation $\dot{v} = a$ for the linear dynamics and $\dot{\omega} = \alpha$ for the angular one. We then keep the chosen accelerations a and/or α constant for TTC calculations. Clearly, for nonzero values of a and/or α, the values of v and ω will be time varying.

6.3. Dynamic analysis

In dynamics-based model, forces for linear acceleration and torques for angular accelerations get involved. The equations are inherently second order due to the nature of Newtonian dynamics. The forces involved are due to the tire-road interactions and involve wheel slips, slip angles, and adhesion coefficients. The differential equations for this model have been described in Section "5.3. Combined longitudinal and lateral dynamics."

In order to perform TTC analysis using the dynamic model, we make the control inputs constant at the initial time, just like for other models. In this case, the control variables are applied linear force and the applied wheel torque (from the engine or a motor, etc.) at the initial time t, which are then held constant for TTC calculations. The setup for TTC analysis using this model is illustrated in **Figure 12**. The center of rotation is now dynamic and changes continuously in general, and unlike in the kinematic case is not obtained by the intersection point of the normal lines, but based on the detailed analysis of the differential equations.

7. Numerical examples and results

In this section we will conduct numerical simulations using the various bicycle models that we have presented for vehicle modeling. Special focus will be on cases that produce false positives and false negatives in standard analysis and hence show the importance of these new models. Vehicle-to-vehicle as well as vehicle-to-static object interactions will be presented.

7.1. Vehicle obstacle example

In this subsection we study vehicle–obstacle interaction problem. By using two different relative placements of the obstacle with respect to the vehicle, we will study specific important scenarios.

7.1.1. Standard analysis

The standard traditional technique for SSM using TTC assumes the velocity at initial time t to remain constant. This has interesting consequences in the two scenarios we present next.

In the two scenarios presented here, the initial state of the vehicle is the same for both cases. However, the obstacle placement is different in the two cases. It is clear that a collision takes place in one case, whereas in the other case there is no estimated collision. Hence, in the case where there is an estimated collision, the TTC value can be calculated.

7.1.2. Kinematic analysis

In the standard technique the initial angular velocity is ignored. However, using the bicycle model, we use both initial conditions, initial velocity, as well as initial angular velocity.

In the two scenarios presented here, the initial state of the vehicle is the same for both cases. However, the obstacle placement is different in the two cases just like in the standard case. It is clear that a collision takes place in one case, whereas in the other case there is no estimated collision (**Figures 13**, **14**). Hence, in the case where there is an estimated collision, the TTC value can be calculated.

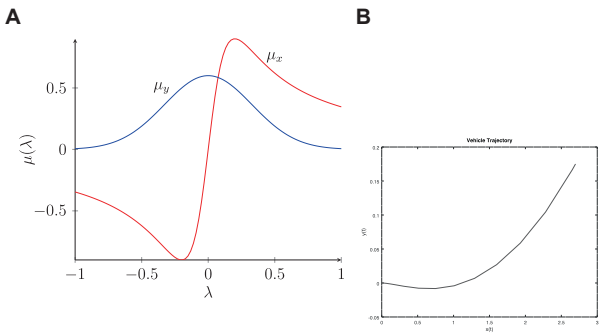

FIGURE 19 | Dry asphalt. **(A)** Road surface condition. **(B)** Trajectory plot.

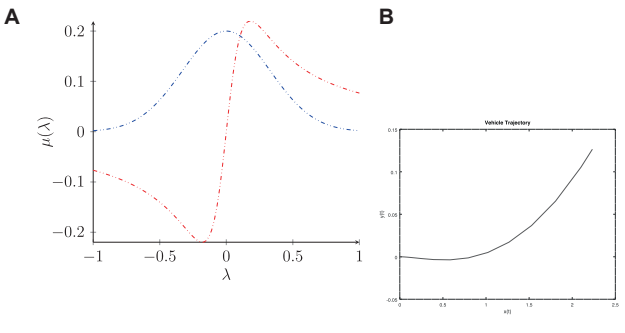

FIGURE 20 | Icy road. **(A)** Road surface condition. **(B)** Trajectory plot.

Figure 15 shows the graphical results of running the differential equations for the model, and then presenting the plots with respect to time.

7.1.3. Comparative analysis of standard and kinematic models

Figure 16 shows the comparative analysis of the standard and the kinematic model cases. It is clear that by ignoring initial angular data, the standard model produces false positive as well as false negative in the two cases.

7.2. Vehicle–vehicle example

In this subsection we consider the case of two vehicles. Even in vehicle–vehicle interaction, the standard technique can produce false positives and false negatives. The analysis method is the same as before. We have non-holonomically constrained differential equations for both vehicles with given initial conditions, and we solve them to produce the estimated trajectories with constant initial conditions on the control variables.

Although we can easily show both false positive and false negative cases, without loss of generality, we will demonstrate the false negative case, i.e., the standard analysis shows no collision (a negative result), which in fact is false, as there would be one.

Figure 17 shows the graphical plots for the results of the numerical simulation performed using the bicycle kinematic models for the two vehicles with the given initial conditions, the visual results of which are shown in **Figure 18**.

7.3. Dynamic analysis

The results in this subsection show that inclusion of road surface conditions change the estimated vehicle trajectories. In most normal road conditions, the results of this model and those of the kinematic model will be very close. However, a vehicle taking a sharp turn in icy conditions can have a very different trajectory when using the kinematic model that ignores the road surface conditions as compared to the results when the dynamic model is used that uses those conditions.

Starting with the same initial conditions used in the numerical examples that we have simulated for standard and kinematic models, we performed numerical simulations for two different road conditions.

First simulation was using dry asphalt whose $\mu - \lambda$ plot is shown in **Figure 19A**. The plots from the numerical simulation results are shown in **Figure 19B**. The second simulation was using icy road conditions whose $\mu - \lambda$ plot is shown in **Figure 20A**. The plots from the numerical simulation results are shown in **Figure 20B**. The effect of the changing road conditions on the details of the trajectories can be seen in the plots shown in these figures.

8. Conclusion

This paper has shown that standard surrogate safety measures that only extend linear current velocities can produce false positives and negatives. We have proposed a bicycle model-based analysis of vehicle trajectories to improve the analysis for safety surrogates using a kinematic model that uses non-holonomically constrained dynamic equations as well as a model that takes road tire adhesion into consideration in the analysis of vehicle movements.

References

1. Arun A, Haque MM, Bhaskar A, Washington S, Sayed T. A systematic mapping review of surrogate safety assessment using traffic conflict techniques. *Accident Anal Prev.* (2021) 153:106016.
2. Castillo E. *Extreme Value Theory in Engineering.* Amsterdam: Elsevier (2012).
3. Chen C-T. *Linear System Theory and Design.* Oxford: Oxford University Press (2012).
4. De Haan L, Ferreira A, Ferreira A. *Extreme Value Theory: An Introduction.* (Vol. 21). Cham: Springer (2006).

5. Goldstein H, Poole C, Safko J. *Classical Mechanics Addison-Wesley*. Reading, MA: Addison-Wesley (1980). 426 p.
6. Isidori A. *Nonlinear Control Systems: An Introduction*. Cham: Springer (1995).
7. Jazar RN. *Vehicle Dynamics*. (Vol. 1). Cham: Springer (2008).
8. Kachroo P, Rao KR. 2d curve analysis based development of safety surrogate measures in lane-free heterogeneous traffic. *Proceedings of the 14th International Conference on Transportation Planning and Implementation Methodologies for Developing Countries (TPMDC)*. Bombay: Indian Institute of Technology Bombay (2022a).
9. Kachroo P, Rao KR. Tire road surface conditions and 2d curve analysis based development of surrogate safety measures. *BOHR Int J Eng.* (2022b) 1:1–9.
10. Kachroo P, Tomizuka M. *Vehicle Traction Control and Its Applications. California PATH Research Paper*, UCB-ITS-PRR-94-08(ISSN 1055-1425). California: PATH (1994). p. 3–44.
11. Kiencke U, Nielsen L. *Vehicle Modelling*. Cham: Springer (2005).
12. Lin J-S, Ting W-E. Nonlinear control design of anti-lock braking systems with assistance of active suspension. *IET Control Theory Appl.* (2007) 1:343–8.
13. Luca AD, Oriolo G, Samson C. Feedback control of a nonholonomic car-like robot. In: Laumond J-P editor. *Robot Motion Planning and Control*. Berlin: Springer (1998). p. 171–253.
14. Nadimi N, Ragland DR, Mohammadian Amiri A. An evaluation of time-to-collision as a surrogate safety measure and a proposal of a new method for its application in safety analysis. *Transport Lett.* (2020) 12:491–500.
15. Ozbay K, Yang H, Bartin B, Mudigonda S. Derivation and validation of new simulation-based surrogate safety measure. *Transport Res Record.* (2008) 2083:105–13.
16. Pacejka H. *Tire and Vehicle Dynamics*. Amsterdam: Elsevier (2005).
17. Sastry S. *Nonlinear Systems: Analysis, Stability, and Control*. (Vol. 10). Cham: Springer Science & Business Media (2013).
18. Shen S, Benedetti MH, Zhao S, Wei L, Zhu M. Comparing distance and time as driving exposure measures to evaluate fatal crash risk ratios. *Accident Anal Prev.* (2020) 142:105576.
19. Taheri S, Law EH. Investigation of a combined slip control braking and closed loop four wheel steering system for an automobile during combined hard braking and severe steering. *Proceedings of the 1990 American Control Conference*. San Diego, CA: IEEE (1990). p. 1862–7.
20. Tarko A. *Measuring Road Safety with Surrogate Events*. Amsterdam: Elsevier (2019).
21. Zabczyk J. *Mathematical Control Theory*. Cham: Springer (2020).